POLITECNICO DI TORINO
Repository ISTITUZIONALE

Design Comparison of Wrapped and non-Wrapped Interior Permanent Magnet Synchronous Machines

Original
Design Comparison of Wrapped and non-Wrapped Interior Permanent Magnet Synchronous Machines / Acquaviva, R., Ferrari, S., Silvagni, M., Tonoli, A., Pellegrino, G.. - ELETTRONICO. - (2024), pp. 1-6. (2024 International Conference on Electrical Machines (ICEM) Torino 01-04 September 2024) [10.1109/icem60801.2024.10700321].

Availability:
This version is available at: 11583/2993316 since: 2024-10-10T21:05:46Z

Publisher:
ieee

Published
DOI:10.1109/icem60801.2024.10700321

Terms of use:

This article is made available under terms and conditions as specified in the corresponding bibliographic description in the repository

Publisher copyright
IEEE postprint/Author's Accepted Manuscript

©2024 IEEE. Personal use of this material is permitted. Permission from IEEE must be obtained for all other uses, in any current or future media, including reprinting/republishing this material for advertising or promotional purposes, creating new collecting works, for resale or lists, or reuse of any copyrighted component of this work in other works.

(Article begins on next page)

18 November 2026

Design Comparison of Wrapped and non-Wrapped Interior Permanent Magnet Synchronous Machines

Roberto Acquaviva
Energy Department "Galileo Ferraris"
Politecnico di Torino
Turin, Italy
roberto.acquaviva@studenti.polito.it

Simone Ferrari
Energy Department "Galileo Ferraris"
Politecnico di Torino
Turin, Italy
simone.ferrari@polito.it

Mario Silvagni
Dept. of Mechanical and Aerospace Eng.
Politecnico di Torino
Turin, Italy
mario.silvagni@polito.it

Andrea Tonoli
Dept. of Mechanical and Aerospace Eng.
Politecnico di Torino
Turin, Italy
andrea.tonoli@polito.it

Gianmario Pellegrino
Energy Department "Galileo Ferraris"
Politecnico di Torino
Turin, Italy
gianmario.pellegrino@polito.it

***Abstract*—Wrapped Interior Permanent Magnet (IPM) synchronous motors represent a recent breakthrough in the domain of high-speed IPM machines. This innovative rotor design introduces buried Permanent Magnets (PMs) and a Carbon-Fiber (CF) sleeve to secure the magnets against centrifugal forces, obviating the need for traditional iron bridges or ribs, typical in conventional IPM rotor configurations. Nevertheless, the design and analysis of retaining sleeves are essential for enabling safe and efficient high-speed operation. This paper proposes an analytical model for the retaining sleeve design, introducing a graphical pre-design tool to forecast the dimensions and characteristics requisite for the carbon sleeve, given the target maximum speed. A comparative analysis is then conducted between standard IPM motors with ribs and wrapped IPM motors at different maximum speed speeds, highlighting the benefits of the wrapped IPM design and the possible drawbacks.**

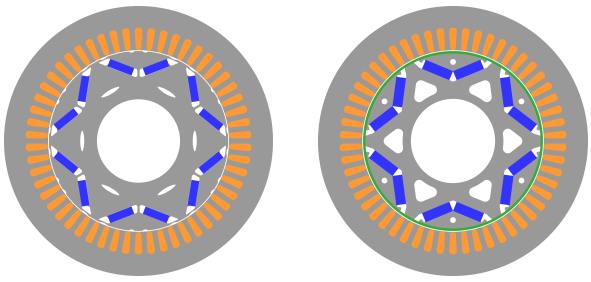
***Index Terms*—High-Speed Electrical Machines, Electrical Machines Design, Permanent Magnet Synchronous Motors**

I. Introduction

The electric automotive industry has witnessed a remarkable growth in recent years, driven by the increasing demand for efficient and sustainable energy solutions. In the last decade, several academic and industrial research groups invested a huge amount of resources in the electric or hybrid powertrain development, launching several models to compete in the e-Mobility market [1].

Electric motors play a pivotal role in the automotive industry's transition towards sustainable and high-performance vehicles. However, optimizing their design for superior efficiency and performance remains a complex challenge.

One of the strategies to increase the power density is the adoption of high-speed motors, with the maximum speed that, in the last powertrain, reaches 20000 rpm [2]. High-speed electrical machines have been developed and used for a long time. One advantage of high-speed electric machines is their ability to reduce system weight for a given level of power conversion [3]. This reduction in weight is crucial in traction applications where lighter components translate to a lower overall load and higher vehicle efficiency. However, in the automotive context, space is often even more critical than weight. To meet customer expectations for comfort, increased battery capacity for extended autonomy, and additional components, a compact motor becomes essential. More specifically, the volumetric power density of an electrical machine is improved when the volume is reduced at a constant torque and speed. Alternatively, speed must be increased to compensate for decreasing torque [4]. Nonetheless, achieving high-speed motor operation presents numerous design challenges. Attention must be devoted to mechanical strength, vibration control, and the mitigation of energy losses. High-speed rotation generates significant centrifugal forces, which means high mechanical stress and deformation in motor components. Therefore, the design of bearings and rotor assemblies must account for these forces to prevent premature failure or imbalance-induced vibrations. Typically, V-type IPM motors with structural ribs are adopted for high-speed traction motors. The popularity of this particular lamination geometry can be attributed to its excellent mechanical retention properties, that ensures the



(a) (b)

Fig. 1. Cross sections of two examples traction motor from a) Tesla Model 3 (standard ribs IPM motor) and b) Tesla Model S Plaid (wrapped IPM motor).

secure fixation of the permanent magnets within the rotor structure. However, the presence of iron ribs short-circuit part of the PM flux, reducing the net PM flux linkage that crosses the airgap. This detriment has two main drawbacks. First, the peak torque of the motor is reduced, because of the lower PM flux linkage. Second, the characteristic current of the motor is reduced, causing a reduction of the power asympthote at high speed, with an even more critical issue. An example of actual V-type IPM motor with ribs, adopted in commercial vehicle (Tesla Model 3) is reported in Fig. 1a. Due to the centrifugal force acting on the magnets and on the outer part of the rotor yoke, the thickness of the rib and the two bridges increases with the maximum rotor speed. Besides the higher maximum speed, thicker ribs and bridges increase the flux leakage, causing a reduction of the net PM flux linkage and ultimately a peak torque and power detriment. In order to increase the speed of this motor type without performance detriment, an optimal solution is given by the wrapped IPM motors, where the structural ribs are removed and the structural integrity is guaranteed by a sleeve (typically made of carbon-fiber). In such way, the PM flux linkage is not short-circuited by the iron, but the magnetic airgap must increase. The most widely adopted application of sleeves in electric motors is prominently observed in high-speed Surface Permanent Magnet (SPM) motors. This technology is widely used for small motors thanks to its high power density and its simple structure. The design and analysis of wrapped SPMs have been deeply investigated by several authors [5]. The key of the structural integrity of wrapped SPM motors is the compression that the sleeve gives to the PMs against the rotor back iron. For this reason, the manufacturing process of wrapped rotors is critical, since a well defined pre-stress must be applied, function of the rotor geometry and the aimed maximum speed, as well as the structural properties of the materials.

Besides the high power density and the high speed, wrapped SPM motors are not optimal for traction applications, mainly because of the bad field-weakening operation of these motors, that is needed to limit the inverter size and have high efficiency on a wide speed range. Then, SPM motors are typically weak against irreversible PM demagnetization, that can occur for high current loading and temperatures. However, their simple geometry allows the development of several analytical models for the sleeve design and evaluation, that results also quite accurate. A good solution for the high-speed traction motor is represented by the wrapped IPM motors, that merges the design advantages of IPM motors (as good field-weakening capability, good torque and power density and good demagnetization immunity) with the benefit of the sleeve, that cancel the flux leakage drained by the structural ribs. An example of this solution is the recent traction motor of the Tesla Model S Plaid [6], shown in Fig. 1b, that presents a standard V-type IPM cross-section, with a rib-less design and a retaining sleeve that guarantees the structural integrity, even at higher speeds that the ribbed-IPM motor counterpart (represented by the Tesla Model 3 motor).

This paper proposes an insightful method for the design of wrapped-IPM (WIPM) motors, with the focus on the structural part. The novel sleeve designer plane will be introduced as graphical design method, based on analytical models previously validated with Finite Element Analysis (FEA) simulations [7]. Then, motors for three different maximum speeds will be designed, both with classical IPM rotor with structural ribs and employing the proposed wrapped-IPM topology, for a total of six designs. The comparison on electromagnetic and structural performance of these motors will highlight advantages and drawbacks of the wrapped designs over the standard solution with ribs, relating the comparison also with the maximum design speed. Last, the proposed sleeve designer procedure is included in SyR-e [8], an open-source environment for electric motor design and analysis, improving also the parametrization and description of the wrapped-IPM motors.

II. Sleeve Design for Wrapped IPM Motors

A. Analytical Model for Sleeve Analysis

The sleeve stress computation is tackled in an analytical way, in order to reduce the computational effort. The analytical formulation of Wrapped IPM motor was presented in [7]. Here, it is reviewed and implemented into a parametric study, in order to simplify the sleeve design in terms of thickness and pre-stress. The analytical model is based on a simplified geometry, obtained as in Fig. 2.

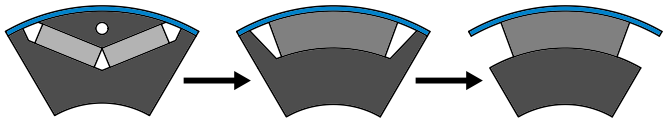


Fig. 2. Geometry transformation from the actual lamination to the simplified geometry for the analytical model [7].

Three rings are present in the final geometry: an outer ring, modeling the sleeve (index 1 in the formulation), an equivalent ring for PMs and pole piece, identified with the index 2 and an inner ring, modeling the rotor back yoke (index equal to 3). The structural properties of the three layers are obtained as explained in [7].

The dimension and stress definitions of the equivalent geometry are reported in Fig. 3. It is worth noting that the key parameters are the one related to the sleeve, that is the layer #1 and it is the same for both the actual geometry and the simplified model.

The formulation of the analytical model is divided into two main operating areas, divided by the pole lift-off condition. For low speed, the pre-stress applied to the sleeve will push the second layer (PMs and pole piece) to the rotor back iron. As speed increases, the centrifugal force contrasts the sleeve pre-stress and, at a certain speed, the second layer will detach from the pole piece. This is defined the lift-off speed and it is set as speed costraint for the safe operation of wrapped IPM motors. The main sleeve design quantities are represented and summarized in Fig. 4a. The colored curves represents the tangential stress in the sleeve σ_{t1} function of the rotor speed,

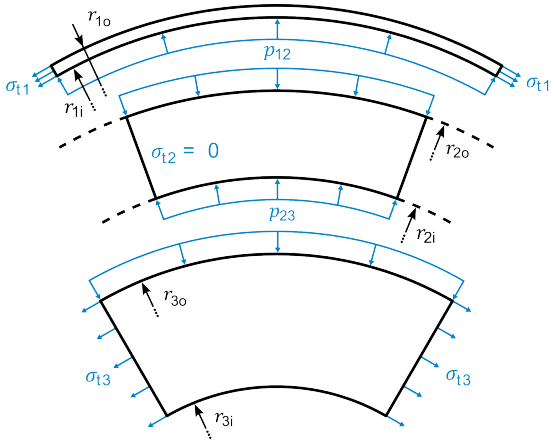
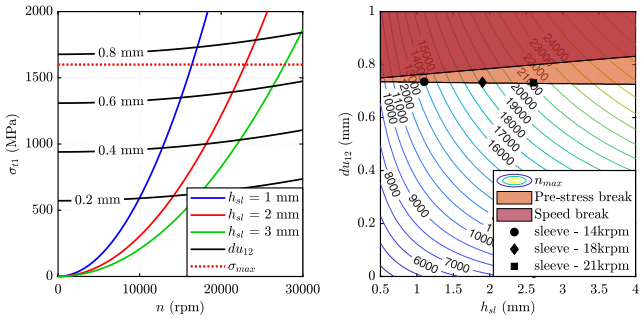


Fig. 3. Parameters definition of the simplified geometry [7].

evaluated for various sleeve thickness h_{sl} values and zero pre-stress. Furthermore, the black curves represent the sleeve stress for different sleeve interference du_{12} values, on this plane evaluated for a single average sleeve thickness and directly related with the approximated pre-stress.

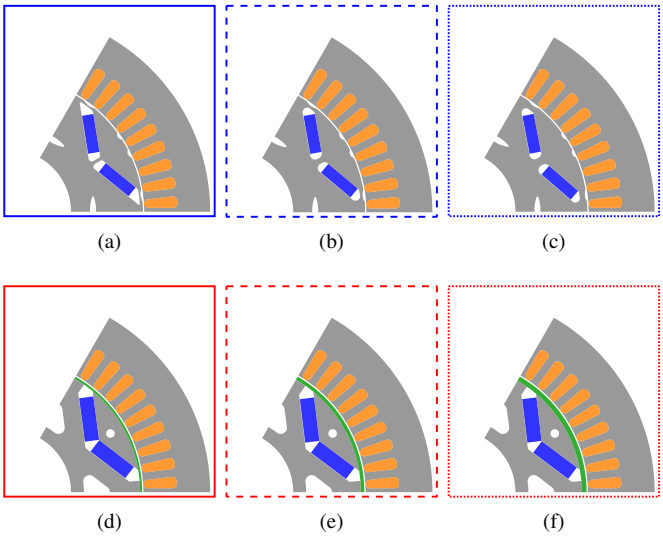
The crossing between the black curves and the colored curves identify the lift-off speed for the considered sleeve thickness and sleeve interference. For speed lower than the lift-off speed, the stress in the sleeve will follow the black line, while for speed higher than the lift-off speed, the sleeve tangential stress will follow the colored line.



(a) (b)

Fig. 4. Sleeve Designer plane: a) explicit form, with tangential stress function of the rotor speed for different sleeve thickness and interferences and b) final form of the sleeve designer plane: contours of maximum speed function of the sleeve thickness and the interference.

To design the wrapped IPM motors avoiding to approximate the pre-stress for a single average sleeve thickness, a sleeve designer plane is computed. It is reported in Fig. 4b and reports the lift-off speed (i.e. the maximum motor speed) function of the sleeve thickness and the interference. Two colored areas are identified on the plane. The speed break area, colored in red, identifies the (h_{sl}, du_{12}) combinations that, with the pre-stress caused by the interference alone, have a sleeve stress higher than the sleeve maximum stress. The other highlighted area is colored in orange and identified as pre-stress break area



(a) (b) (c)

(d) (e) (f)

Fig. 5. Cross sections of the six compared motors: a) 14 krpm IPM motor, b) 18 krpm IPM motor, c) 21 krpm IPM motor, d) 14 krpm WIPM motor, e) 18 rrpm WIPM motor and f) 21 krpm WIPM motor.

and identifies all the (h_{sl}, du_{12}) combinations that have a lift-off speed at stress higher than the maximum sleeve stress. At the end, the optimal point for the sleeve design lies along the boundary between the danger area and the non-danger area. For these points, the sleeve thickness, and so the magnetic airgap thickness, are minimized, allowing high torque and power density.

III. Design Comparison

To assess the advantages and disadvantages of the wrapped IPM motors, three different target speeds are considered and a total of six motors are designed and compared. For each speed, a wrapped-IPM version and a standard IPM with ribs are designed. The cross-sections of the six motors are reported in Fig. 5. The motors share the same stator as well as the same inverter (400 Vdc and 800 Apk). The wrapped IPM motors have slightly thicker PMs than the standard IPM motors thanks to the higher space in the rotor due to the absence of the ribs. Increasing the speed, the ribs thickness (both for radial and tangential sections) increase, with a detriment of the magnetic performance that will be assessed later. On the other hand, WIPM machines present thicker sleeve thickness for higher speeds.

A. Flux Maps

The first term of comparison are the flux maps. The limit curves without cross-saturation effect are reported in Fig. 6. Dealing with the d axis flux linkage, the effect of the increasing speed is significantly more evident for ribs IPM motors. Indeed, the PM flux linkage reduction with speed is about 30% for IPM motors with ribs, while it is just 14% for wrapped IPM motors. Furthermore, the inductance (i.e. the slope of the flux linkage curve) is higher for ribs motors, because of the flux leakage through the structural ribs, even if the magnetic

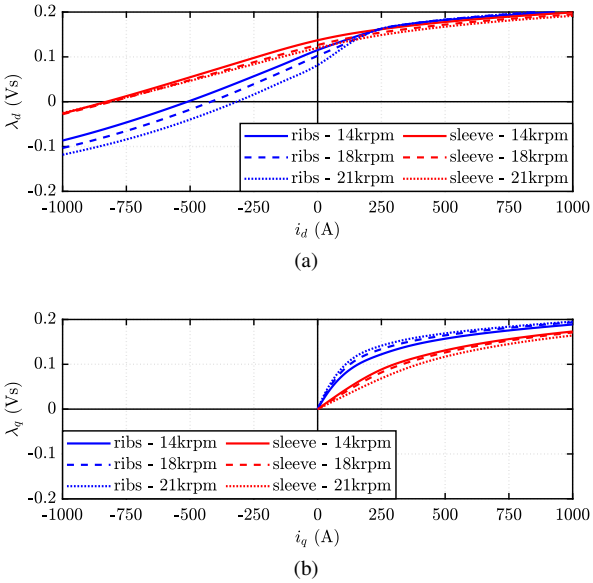


Fig. 6. Flux maps curves without cross-saturation of the six motors: a) $\lambda_d(i_d)$ and b) $\lambda_q(i_q)$

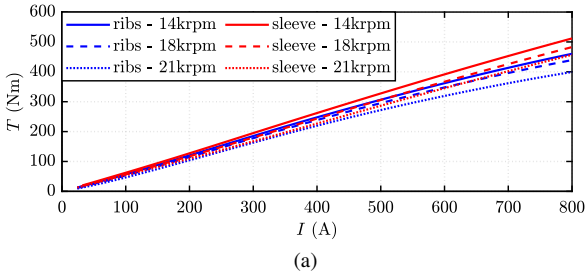


Fig. 7. MTPA curves comparison: torque versus current curves for the six machines

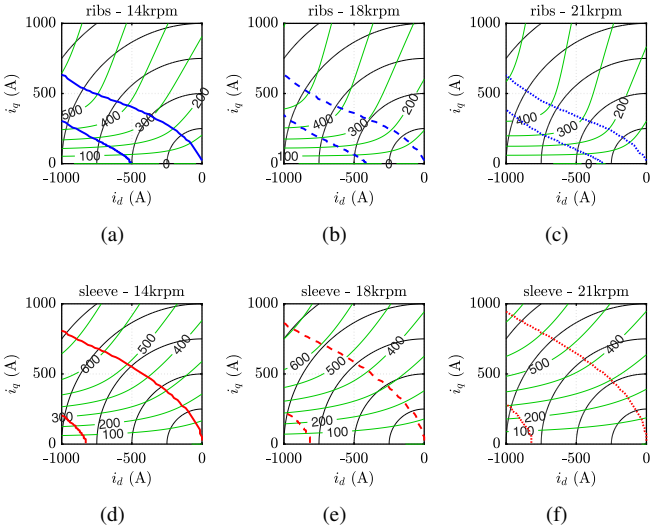


Fig. 8. MTPA and MTPV trajectories of the six considered motors on the (i_d, i_q) plane.

airgap of these motors is thinner compared to the WIPM versions. This behavior reflects in a higher and more constant characteristic current for wrapped IPM with the maximum speed, that will procduce a better power profile, as will be demonstrated later. The behaviors are opposite on the q axis: for wrapped IPM motors, the speed increase cause a reduction of the q axis flux linkage because of the higher magnetic airgap, that increases with maximum speed. On the other hand, the ribs motors presents increased q axis flux linkage with the speed because of the ribs itself, that helps to guide flux lines along the q axis.

B. Maximum Torque Per Ampere Curves

The comparison continues with the control trajectories and the Maximum Torque per Ampere (MTPA) and Maximum Torque per Voltage (MTPV) curves. The MTPA locus are computed directly from the flux maps and the torque versus current curves are compared in Fig. 7. It is worth noting that the motors with sleeve express in general a higher torque for the same current. Moreover, the torque constant is almost linear for this kind of motors, while for IPM motors with ribs, two saturation areas occurs. The first is at low currents, when the ribs saturation still play a role in the magnetic behaviors of the motor. Last, for very high currents, iron saturation occurs and torque constant decreases. This last aspect is present also for wrapped IPM motors, but becomes relevant for higher currents, outside the inverter limits.

The MTPA and MTPV trajectories of the six motors are reported and compared in Fig. 8. The different weight of the reluctance and PM torque is evident in this comparison. Indeed, the WIPM motors present MTPA curves further away from the $-d$ axis, index of a higher PM torque component. While the IPM motors have MTPA curves that are closer to the d axis and so higher current angles and higher weight of the reluctance torque components. The other relevant difference in this comparison is the MTPV and the characteristic current (i.e. the intersection between MTPV and d axis). The characteristic current is almost the same for the three WIPM motors, while decreases with the speed for the IPM motors, narrowing the operating area on the (i_d, i_q) plane included between the two trajectories and causing a premature MTPV control and power-descending field-weakening.

C. Operating Limits

After the computation of the control trajectories, the operating limits at maximum DC link voltage and phase currents are retrieved and compared in Fig. 9 both in terms of torque and in terms of power. The conclusions done for the torque capability along the MTPA are confirmed here: below the base speed, wrapped IPM motors express a higher torque than IPM motors with ribs. As the maximum speed increases, the peak torque is reduced for both technologies, with a higher degradation for standard IPM motors. The huge differences between the two technologies is the field-weakening area. For IPM motors with ribs, as maximum speed increases, the power at high speed is reduced because of the reduced characteristic current. On the other hand, the characteristic

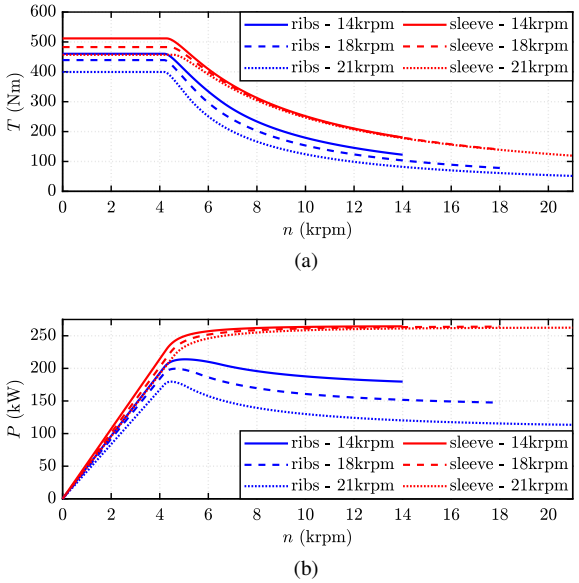


Fig. 9. Operating limits comparison at 400Vdc and 800Apk in loss-less conditions: a) torque versus speed and b) power versus speed.

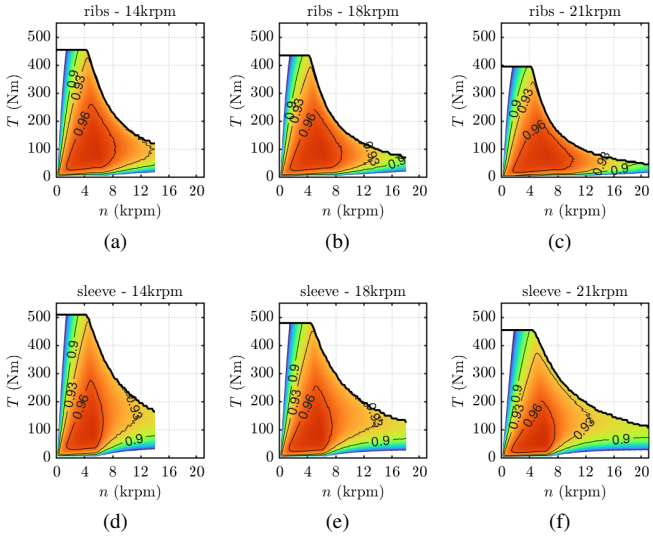


Fig. 10. Efficiency maps of the six motors at 400 Vdc and 800Apk evaluated with winding and PMs at 120°C and 80°C, respectively.

current of the wrapped IPM motor is not affected by the maximum speed, making the torque and power curves at high speed of these motors practically superimposed. Furthermore, the characteristic current of the wrapped IPM motors is equal to the maximum current, resulting in an ideal field-weakening condition and a flat power profile.

D. Efficiency Maps

The efficiency maps of the six machines are computed and compared in Fig. 10. The maximum inverter limits are considered and the motor is set at 120°C and 80°C for windings and PMs. Stator Joule loss, iron loss and PM loss are taken into account, giving as input a sinusoidal supply. The operating limits shown in Fig. 9 are confirmed, with a small discrepancy due to the loss (neglected in the previous analysis). Dealing with the numbers, the comparison highlights the difference between the two technologies. Besides the higher peak performance, both in terms of torque and power, wrapped IPM motors presents a smaller high efficiency area, limited especially at lower speeds (below the base speed). The difference is mainly due to copper loss and the field weakening operation. These are boosted by the increased harmonic content caused by the equivalent "open slots" at the rotor side. This behavior can be worse if PWM loss are considered.

E. Demagnetization Limit and Fault Reaction

A last comparison between the six motors is done in terms of fault reaction and demagnetization. As for automotive standard [9], the safe state of the drive-line is ensured when a system fault is detected in the Active Short Circuit (ASC). This is necessary to avoid high voltages at the inverter and the uncontrolled generator condition (motor voltage higher than DC link voltage). However, ASC induces high currents in the motor, that can irreversibly demagnetize the PMs. The demagnetization curves of the six motors are reported and compared in Fig. 11. The curves express the maximum current that can be injected against the PMs without irreversibly demagnetize more than 1% of the PM volume. These curves are reported function of the PM temperature and normalized by the maximum inverter current. The three curves are almost superimposed for wrapped motors, with demagnetization limits between 4 and 2 times the maximum inverter current (spanning between 20°C and 120°C), while for standard motors, the demagnetization limit is in general higher (especially at low temperatures) and more dependent to the maximum speed. For the rated PM temperature (80°C), the demagnetization limits is around 1600A (2x the maximum current), while for the high-speed ribs motors is more than 4 times the demagnetization limit.

Once the demagnetization limit is identified and the motor flux maps are known, it is possible to compute the peak ASC current in the worst-case pre-fault point [10]. The current waveform after ASC triggers are computed for the six motors and compared in Fig. 12. For reference, the demagnetization limit is reported in black for each motor. The selected pre-

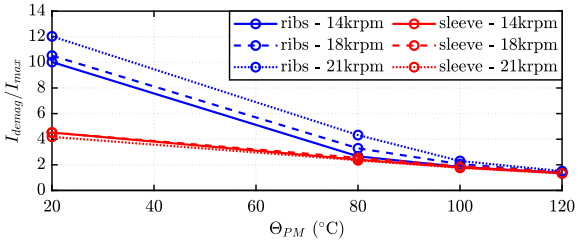


Fig. 11. Demagnetization limit of the six motors function of the PM temperature.

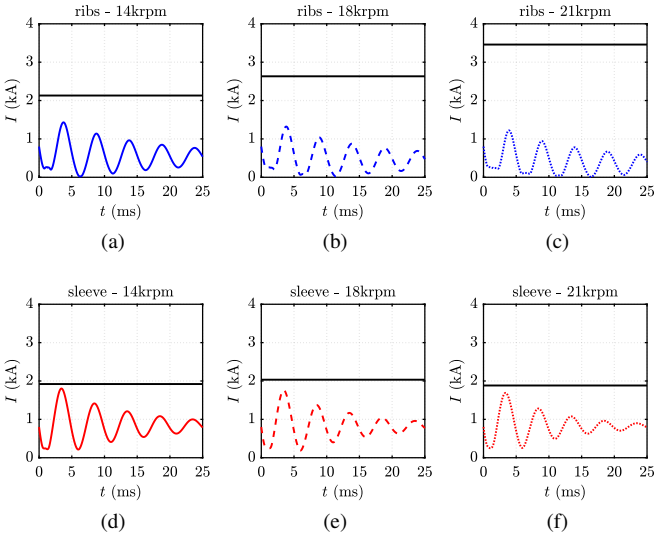


Fig. 12. ASC current amplitude for the 6 motors evaluated at 120°C and 80°C, respectively. Pre-fault condition: 4000rpm 800Apk along the MTPA.

fault operating point is the maximum phase current along the MTPA at 4000 rpm (that is close to the base speed of all the six motors). The PM and winding temperatures are set to 80°C and 120°C, First of all, the difference of the demagnetization limits are more evident here. This limit is almost constant for the wrapped IPM motor and increases with the maximum speed (i.e. the ribs thickness) for standard IPM motors. Dealing with the ASC current, it reduces increasing the speed for the standard IPM motors, that are largely safe against demagnetization. The condition is much more critical for wrapped IPM motors, that presents higher peak currents. This, together with the reduced demagnetization limit, make this motors more critical for the demagnetization problem. However, the analysis tells that the three wrapped IPM motors are safe against demagnetization in the selected condition, even if the margin is very limited.

IV. Conclusions

The paper reviews the design process for wrapped IPM motors for traction application. Furthermore, an insightful graphical design procedure is introduced, helping the design of minimal sleeve thickness for a given speed in seamless time. Then, the proposed sleeve design plane is adopted to design 3 wrapped IPM motors for three different maximum speeds, that are compared with the three standard IPM motors with ribs, designed for the same speeds. An extensive comparison is carried out, highlighting the advantage of the wrapped IPM motor in terms of peak power and field-weakening capability. Indeed, for this kind of motor, the maximum speed increase slightly affect peak torque, without penalizing the peak power and the power in field-weakening operation, as happens for IPM motors with ribs. Besides this crucial advantage, the wrapped IPM motors results slightly more critical in terms of irreversible demagnetization during ASC, that is mandatory for these motors. Last, the efficiency of the six motors are comparable, with a slight advantage of wrapped IPM motors below the base speed.

Acknowledgment

The research has been conducted with the support of Power Electronics Innovation Center (PEIC) of Politecnico di Torino.

References

[1] R. Irle, "Global ev sales for 2022," *EV-Volumes*, 2023. [Online]. Available: https://www.ev-volumes.com/

[2] B. Sarlioglu, C. T. Morris, D. Han, and S. Li, "Benchmarking of electric and hybrid vehicle electric machines, power electronics, and batteries," in *2015 Intl Aegean Conference on Electrical Machines Power Electronics (ACEMP), 2015 Intl Conference on Optimization of Electrical Electronic Equipment (OPTIM) 2015 Intl Symposium on Advanced Electromechanical Motion Systems (ELECTROMOTION)*, 2015, pp. 519–526.

[3] D. Gerada, A. Mebarki, N. L. Brown, C. Gerada, A. Cavagnino, and A. Boglietti, "High-speed electrical machines: Technologies, trends, and developments," *IEEE Transactions on Industrial Electronics*, vol. 61, no. 6, pp. 2946–2959, 2014.

[4] T. Epskamp, B. Butz, and M. Doppelbauer, "Design and analysis of a high-speed induction machine as electric vehicle traction drive," in *2016 18th European Conference on Power Electronics and Applications (EPE'16 ECCE Europe)*, 2016, pp. 1–10.

[5] G. Gallicchio, F. Cupertino, M. Di Nardo, M. Reza Ilkhani, and C. Gerada, "Design methodologies of high speed surface permanent magnet synchronous machines," in *2023 IEEE International Electric Machines Drives Conference (IEMDC)*, 2023, pp. 1–7.

[6] L. E. Olsen, ",et al., permanent magnet motor with wrapping," International Publication Number WO 2021/225902 A1, Nov. 2021.

[7] J. Binder, M. Silvagni, S. Ferrari, B. Deusinger, A. Tonoli, and G. Pellegrino, "High-speed ipm motors with rotor sleeve: Structural design and performance evaluation," in *2023 IEEE Workshop on Electrical Machines Design, Control and Diagnosis (WEMDCD)*, 2023, pp. 1–6.

[8] S. Ferrari and G. Pellegrino, "SyR-e: Synchronous Reluctance (machines) - evolution." [Online]. Available: www.github.com/SyR-e

[9] ISO/TC 22/SC 32, "ISO26262-1:2018." International Organization for Standardization, 2018. [Online]. Available: https://www.iso.org/standard/68383.html

[10] S. Ferrari, G. Dilevrano, P. Ragazzo, P. Pescetto, and G. Pellegrino, "Fast determination of transient short-circuit current of pm synchronous machines via magnetostatic flux maps," *IEEE Transactions on Industry Applications*, vol. 59, no. 4, pp. 4000–4009, 2023.